Numerical modeling of plasma assisted deflagration to detonation transition in a microscale channel

Zhiyu Shi[a], Xingqian Mao[a,*], Andy Thawko[a], Yiguang Ju[a,b]

[a] *Department of Mechanical and Aerospace Engineering, Princeton University, Princeton, NJ 08544, USA*
[b] *Princeton Plasma Physics Laboratory, Princeton, New Jersey 08540, USA*

Abstract

This work numerically studies the plasma assisted deflagration to detonation transition (DDT) of H_2/O_2 mixtures in a microscale channel with detailed chemistry and transport. The results show that the DDT onset time is non-monotonically dependent on the discharge pulse number. The DDT is accelerated with small pulse numbers, whereas retarded with large ones. Two different DDT regimes, respectively at a small and large plasma discharge number, via acoustic choking of the burned gas and plasma-enhanced reactivity gradient without acoustic choking, are observed. Without plasma discharge, pronounced pressure and temperature gradients in front of the flame are generated by acoustic compression after the choking of the burned gas, triggering DDT via autoignition. With small plasma pulse numbers, the plasma-generated species enhance the ignition kinetics and lead to an increased reactivity in the boundary layer. After the choking of the burned gas, the plasma-enhanced reactivity advances the sequence of autoignition near the wall, strengthens ignition-shock wave coupling, and accelerates DDT. However, with a large discharge pulse number, a direct autoignition initiating DDT can occur without the acoustic choking of the burned gas due to the strongly accelerated reactivity and elevated temperature. In this case, DDT onset is retarded because the elevated temperature increases sonic velocity and the increased reactivity accelerated fuel oxidation in front of the flame, decelerating the formation of a leading shock and subsequent pressure buildup ahead of the flame. The present modeling reveals that no matter with or without plasma discharge, DDT is initiated by autoignition in thermal, pressure, and reactivity gradient fields via Zel'dovich gradient mechanism. The acoustic choking of the burned gas may not be the necessary condition of DDT with strong plasma-enhanced reactivity gradient. This work provides an answer to the experimentally observed non-monotonic DDT onset time by plasma, which provides guidance to control DDT in advanced detonation engines and fire safety of hydrogen-fueled catalytic reactors in microchannels by non-equilibrium plasma discharge.

Keywords: Non-equilibrium plasma; Deflagration to detonation transition; Zel'dovich gradient mechanism; Autoignition; Ignition-shock wave coupling

---

*Corresponding author.

1) Novelty and Significance Statement

The novelty of this research is the understanding of plasma assisted deflagration to detonation transition (DDT) mechanism. This work shows the DDT initiation can be accelerated and retarded non-monotonically by using a non-equilibrium plasma discharge. Two different DDT regimes, one via autoignition after acoustic choking of the burned gas and the other via plasma enhanced ignition without acoustic choking of the burned gas, are reported. The present finding is significant because DDT control is pivotal in advanced detonation engines and fire safety of industrial catalytic reactors in microchannels. This work provides a new insight and method to control DDT by using non-equilibrium plasma.

2) Author Contributions

- **Zhiyu Shi:** designed research, performed research, wrote the paper
- **Xingqian Mao:** performed research, wrote the paper, supervision
- **Andy Thawko:** review and editing
- **Yiguang Ju:** review and editing, supervision

3) Authors' Preference and Justification for Mode of Presentation at the Symposium

The authors prefer **OPP** presentation at the Symposium, for the following reasons:

- A room-audience-level discussion with experts in multiple fields including plasma and detonation will be beneficial.
- Past research on detailed plasma-assisted DDT mechanisms is limited.
- This work independently explores acceleration and retardation effects on DDT by non-equilibrium plasma.
- This is the first time that the complete process from plasma, ignition, deflagration to detonation is conducted.
- This work provides a new method to control DDT in advanced engines and hydrogen-fueled catalytic reactors.

1. Introduction

Deflagration to detonation transition (DDT), referring to the transition from subsonic to supersonic combustion waves, has drawn great attention in combustion science over the past decades. This phenomenon is pivotal in the development of advanced pressure-gain combustors such as Rotating Detonation Engines (RDEs) and Pulsed Detonation Engines (PDEs) [1, 2], which can thermodynamically enhance the efficiency by up to 30%. In contrast, in contexts such as engine knocking, chemical-catalytic synthesis, and industrial fire safety [3], DDT poses risks and must be prevented. Consequently, a comprehensive understanding of the DDT mechanism is crucial for both fundamental research and diverse industrial applications.

Previous studies have provided a substantial understanding of the DDT mechanism by different approaches [4-8]. Several mechanisms such as the hotspot mechanism, pressure gradient mechanism, and turbulence driven DDT mechanism have been proposed. Houim et al. [4] showed that the viscously heated flame-wall boundary layer formed hot spots and can be considered as a very long gradient in reactivity. This reactivity gradient initiated detonation across all geometrical configurations and dimensions by simulations. Ivanov et al. [6] found that the pressure peak at the flame front kept increasing due to the positive feedback between the pressure pulse and flame acceleration during deflagration. This pressure peak finally steepened into a shock wave which was strong enough for a detonation wave formation. Poludnenko et al. [8] proposed that the turbulent burning speed exceeding a Chapman-Jouguet (C-J) deflagration velocity should be a critical condition for turbulence-induced DDT. Under this condition, the burned and unburned gases were both choked, instigating a turbulent compressible flame runaway and further DDT. With these previous studies, a consensus has emerged regarding the coupling of flame dynamics, shock waves, and autoignition in DDT. Although many studies of DDT have been conducted, there are still some debates about DDT mechanisms.

To accelerate DDT onset in microchannels, the thermal and kinetic enhancements have been explored in previous studies [9, 10]. The results showed that the ozone addition significantly accelerated DDT onset via kinetic enhancement. The O radical decomposed by ozone overcomes the rate-limiting step $H + O_2 = OH + O$, which reduces the induction length and shortens the ignition delay time, further kinetically enhancing DDT. Due to the efficacy of kinetic enhancement in reducing ignition delay time, lowering minimum ignition energy, extending flammability limits, and promoting cool flame chemistry [11-13], the application of non-equilibrium plasma on DDT has drawn great attention [14, 15]. The volumetric chemically-active species generated by plasma, such as vibrationally and electronically excited species, radicals, ions, and electrons, can induce pronounced ignition-shock wave coupling by ignition enhancement. Meanwhile, the gas heating and fuel oxidation acceleration by plasma discharge can also affect reaction rates, acoustic speed, and flow choking conditions. Vorenkamp et al. [16, 17] experimentally studied the kinetic enhancement by nanosecond dielectric barrier discharge (ns-DBD) plasma on dimethyl ether/oxygen/argon DDT. The results revealed that plasma discharge non-monotonically affected the DDT onset time and distance. A moderate number of plasma discharge pulses before ignition accelerated low-temperature fuel oxidation, shortened ignition delay, and reduced DDT onset time. However, DDT was retarded by applying excessive pulses due to a reduced heat release rate after partial fuel oxidation before ignition. Therefore, non-equilibrium plasma can be applied to control DDT. Although these experimental studies demonstrated the potential of non-equilibrium plasma to control DDT, the underlying mechanism of plasma assisted DDT and the role of plasma assisted ignition have not been explored.

Motivated by the above discussions, in this work the plasma assisted DDT mechanism is studied by numerical modeling. Firstly, the effects of plasma on DDT onset time are investigated. Secondly, the mechanisms of plasma assisted DDT under varying pulse numbers are discussed by examining the interactions among reaction fronts, shock waves, and boundary layers. Particular attention is focused on the critical conditions leading to DDT. The key factors contributing to DDT with different discharge pulse numbers are studied. Lastly, a comprehensive DDT mechanism applicable to all conditions is proposed and discussed.

2. Numerical methods

Similar to the work of Vorenkamp et al. [16, 17], the configurations for the numerical modeling of plasma assisted DDT are shown in Figure 1. For simplicity, the plasma discharge simulations and the DDT simulations are conducted separately in this work. It is assumed that plasma is uniformly distributed across the channel. A zero-dimensional (0-D) model is used with different number of pulses generated by a repetitively-pulsed nanosecond discharge in the plasma discharge simulations. The discharge simulations are terminated before the subsequent discharge to allow the plasma chemistry to proceed. Then, the temperature and species concentrations obtained after the last discharge pulse are used as input for the DDT simulations. A spark ignition is applied on the left end of the channel to generate the initial ignition kernel.

In the plasma discharge simulations, the time evolutions of species densities and temperature are calculated by a 0-D hybrid ZDPlasKin-CHEMKIN model [18, 19]. The detailed governing equations and validations can be found in previous studies [18, 19].

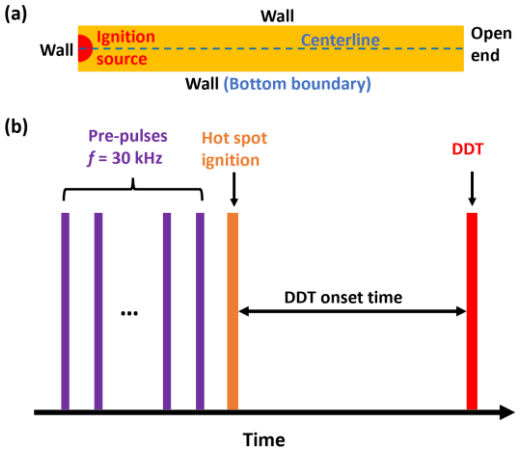

Fig. 1. (a) Schematic of the configuration, and (b) timing sequence of plasma discharge, hot spot ignition and DDT in the numerical simulation.

The H_2/O_2 plasma-combustion kinetic model validated by *in-situ* and *ex-situ* measurements from [19] is used in this work. The plasma kinetic sub-model consists of reactions involving vibrationally excited species $H_2(v=1\text{-}3)$, $O_2(v=1\text{-}4)$; electronically excited species $O_2(a^1\Delta_g)$, $O_2(b^1\Sigma_g^+)$, O_2^*, $O(^1D)$, $O(^1S)$; ions H^+, H_2^+, H_3^+, O^+, O_2^+, O_4^+, OH^+, H_2O^+, H_3O^+, H^-, O^-, O_2^-, O_3^-, O_4^-, OH^-; and electrons. For the combustion sub- mechanism, an updated H_2/O_2 HP-mech [20] is used.

For DDT simulations, a two-dimensional (2-D) multi-scale adaptive reduced chemistry solver (MARCS) [21] developed at Princeton University is used. MARCS is a parallelized solver with adaptive mesh and has been applied for efficient modeling of unsteady, multi-component and compressible reactive flow with detailed chemistry and transport. The TRANSPORT package [22] is utilized to obtain mixture-averaged transport properties. To efficiently handle these properties, the correlated dynamic adaptive chemistry and transport (CO-DACT) method [23] is coupled with the hybrid multi-timescale (HMTS) method [24]. The finite volume method is used to discretize the computational domain. The convection term in the Navier-Stokes equations is constructed using a third-order advection upstream splitting method with pressure wiggles (AUSMPW+) scheme [25] to accurately capture shock waves in high-speed flows. The detailed governing equations and numerical schemes are described in [21]. The excited and charged species with concentrations below 1 ppm after discharge pulses are neglected. The reactions of $H_2(v=1)$, $O_2(v=1)$, $O_2(a^1\Delta_g)$, and O_3 are incorporated in the HP-Mech for DDT modeling.

All the calculations are conducted in a stoichiometric H_2/O_2 mixture (0.667 H_2/0.333 O_2) at 300 K and 1 atm. Simulations of plasma assisted DDT with various pulse numbers (n = 250, 500, 750, 1200) are compared with DDT in the absence of plasma. The discharge frequency is 30 kHz, and the discharge energy in each pulse is 0.2 mJ/cm^3. The reduced electric field E/N (where E is the electric field, N is the gas number density) is 200 Td at which the dissociation of H_2 and O_2 by electrons is efficient [19]. The discharge duration of each pulse is controlled by maintaining a constant energy deposition in the plasma across all simulations. For the DDT simulations, the microscale channel is 1 mm in width and 600 mm in length. The minimum mesh size is 2 µm, equating to 25 grid points over the flame thickness, which suffices to capture key features of flame acceleration and DDT. The initial mixture composition for DDT and mesh size configuration based on the grid refinement study are provided in the Supplementary material. A semicircle hot spot with a temperature of 3000 K at the left boundary is used to initiate ignition and flame propagation. The right end of the channel is set as a transparent boundary. The rest of the boundaries are set as non-slip, reflective, and adiabatic walls.

3. Results and discussion

3.1 Effects of plasma discharge on DDT onset time

To understand the effects of plasma-enhanced reactivity and discharge pulse number on the DDT, the time evolutions of species concentrations and temperature in a single nanosecond discharge by 0-D modeling are presented in Figure 2. During the nanosecond discharge, electrons increase exponentially by electron impact ionization. The excited species and radicals are produced through electron impact excitation and dissociation reactions, such as $e + H_2 \rightarrow e + H_2(v=1)$, $e + H_2 \rightarrow e + H + H$, and $e + O_2 \rightarrow e + O + O/O(^1D)$. At the same time, a rapid temperature increase is observed in the discharge mainly contributed by the Franck-Condon effects in this uniform plasma modeling [26, 27]. The Franck-Condon effects indicate the enthalpy change caused by electron impact dissociations [26]. In the early afterglow stage, the mole fraction of $O(^1D)$ decreases within 10 ns via $O(^1D) + H_2 \rightarrow O + OH$. This promotes the production of O and OH as well as fast gas heating. In the later stage of afterglow, the electron concentration decreases via recombination with ions and attachment reactions. The O, H and OH radicals are consumed through chain-branching and chain-propagation reactions, accelerating the H_2 oxidation and increasing the temperature. Due to the O and H production by plasma discharge, the concentrations of O_3 and HO_2 increase via $O + O_2(+M) = O_3(+M)$ and $H + O_2(+M) = HO_2(+M)$. The production of HO_2 further contributes to H_2O_2 production via $HO_2 + HO_2 = H_2O_2 + O_2$. Fig. 2 also shows that $H_2(v=1)$, $O_2(v=1)$ and $O_2(a^1\Delta_g)$ have longer lifetimes due to slow quenching and relaxation, which will accelerate ignition during DDT. Therefore, by applying different discharge pulses, the plasma will increase the reactivity and change the product

compositions and temperature of the H_2/O_2 mixture, thus affecting the DDT.

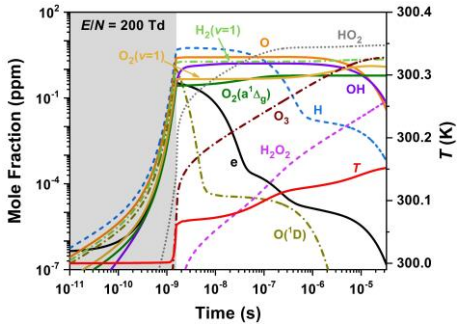

Fig. 2. The time evolutions of species concentrations and temperature in a nanosecond discharge pulse. The grey region represents the discharge stage (~1.56 ns), and the white region represents the afterglow stage.

Figure 3 shows the time histories of the flame propagation velocity during DDT without plasma and with plasma at different discharge pulse numbers. The results show a non-monotonic dependence of the DDT onset time on the discharge number, as summarized in Table 1. With the increase of pulse number, n, the DDT onset time first decreases and reaches the lowest at n = 250, indicating the acceleration of DDT by plasma discharge. The DDT onset time is reduced by 44 μs at n = 250 compared to the case without plasma. Further increase of n to 500 results in a slightly retarded DDT onset time, which is still shorter than the condition without plasma. However, the DDT onset time increases by 154 μs at n = 1200. This non-monotonic relationship between the DDT onset time and the pulse number agrees well with the previous experiments of Vorenkamp et al. [16, 17]. Therefore, the present modeling provides evidence that this non-monotonic behavior is universal for plasma assisted DDT regardless of the fuel. As will be discussed later, the plasma assisted kinetic enhancement by small pulse numbers dominates the DDT acceleration. The plasma-generated chemically active species such as $H_2(v=1)$, O_3, HO_2 and H_2O_2 facilitate autoignition before DDT. Despite the strong enhancement of mixture reactivity with a large pulse number, the large amount of fuel consumption and the increase of the sonic speed due to the increase of temperature increases sonic velocity both decelerate the formation of a leading shock and the necessary pressure buildup ahead of the flame, thereby delaying DDT onset.

It is noted that the pulse number for decreasing DDT onset time was reported as 30-50 in [16], whereas it is 500-750 in the current simulation. Additionally, the simulated DDT time is 600-800 μs, compared to around 100 μs in [16]. This discrepancy arises from differences in discharge conditions, fuel, and the limitations of 2-D modeling. For simplicity, a constant reduced electric field and discharge energy per pulse are used in the 0-D modeling. The discharge energy is smaller than in the experiments due to the difference in voltage waveform, resulting in different optimal pulse numbers. Regarding fuel, H_2/O_2 is more reactive than $DME/O_2/Ar$ used in [16, 17], leading to a higher flame speed and shorter DDT onset time. 3-D DDT simulations capture more realistic autoignition due to complex interactions between the flame front and shock waves [4, 6], making them necessary for accurate comparison with experiments. However, the 2-D simulations tend to severely over-predict the onset time [4, 6], leading to the longer DDT onset time in H_2/O_2 mixtures.

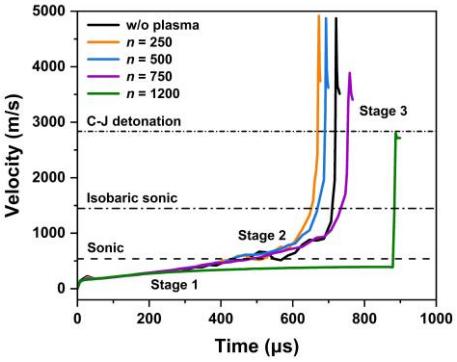

Fig. 3. Time evolutions of flame propagation velocity with plasma at different discharge pulse numbers and without plasma.

Table 1
Initial temperature and DDT onset time without plasma and with plasma at different discharge pulse numbers.

Pulse number	Initial temperature (K)	DDT onset time (μs)
0	300	732
100	319	706
250	353	688
400	394	704
500	425	708
750	518	774
1200	810	886

Fig. 3 shows that except for n = 1200, the time evolution of the velocity follows a similar trend, which can be subdivided into three stages. It is noted that the sonic velocity and isobaric sonic velocity are calculated using the temperature, molecular weight, and the heat capacity ratio of the unburnt gas and burnt gas, respectively. These values differ from those in [16] due to the use of different fuels and conditions. In Stage 1, the flame propagation velocity increases roughly linearly due to the flame area stretching in the boundary layer [28]. In Stage 2, the acoustic choking of the unburned gas occurs when the flame propagation speed exceeds the sonic velocity. A leading shock is then formed and increases the pressure and temperature ahead of the flame, leading to a further acceleration of the flame propagation. However, the strengthening leading shock

compresses the unburned gas in front of the flame and reduces flame propagation speed, leading to flame velocity oscillations and slowdown of flame acceleration. When the flame propagation velocity reaches the isobaric sonic velocity in Stage 3, the burned gas is choked, and flame acceleration generates continuous pressure waves. After that, autoignition occurs and the deflagration abruptly transits to detonation and results in an overdriven detonation speed higher than the C-J velocity. Interestingly, Fig. 3 shows that at n = 1200, flame propagation is significantly slower, and only Stages 1 and 3 are observed. This occurs because the increased sonic velocity at a higher initial temperature inhibits leading shock formation. Consequently, both the leading shock wave and sonic choking in the burned gas are absent. The flame propagation transitions directly to detonation by autoignition (from Stage 1 to 3) without reaching the burned gas choking condition. The detailed mechanism will be discussed in Section 3.2.

3.2 Plasma assisted DDT mechanism

To study the mechanism of plasma discharge on DDT, three cases in Fig. 3 are compared, i.e., without plasma, DDT acceleration at n = 250, and DDT retardation at n = 1200. Figure 4 shows the time evolutions of temperature (T) during DDT. Figs. 4(a) and (b) both show the Zel'dovich–von Neumann–Döring (ZND) detonation wave structure for the cases without plasma and at n = 250, which has a precursor shock wave (I), an induction (II) zone and a reaction (III) zone with the burned gas at the acoustic choking condition. However, for n = 1200 (Fig. 4c), neither the burned gas choking condition nor a leading shock wave exists and only the plasma enhanced reaction zone with strong reactivity gradients is observed.

Without plasma, the accelerating flame acts like a piston which compresses and preheats the unburned mixture between the flame and the precursor shock. The pressure distribution at the centerline in Figure 5(a) shows that the pressure gradient near the flame front increases with time (from t_1 = 730.7 μs to t_2 = 731.4 μs). This continuous compression results in a significantly higher pressure and temperature as well as their gradients ahead the flame front. Therefore, the flame is further accelerated, and the induction zone length reduces, leading to the generation of more intense pressure waves, which is also evident from the pressure profile in Figure 6. This positive feedback enhances the pressure exponentially. At t_3 = 731.8 μs, an ignition is initiated in the region with elevated temperature and pressure gradients after the choking of the burned gas, as shown in Figs. 4(a) and 5(a). The autoignition kernel at the flame front propagates in both forward and backward directions at a supersonic speed with a Mach number of 2.6 and initiates a strong shock wave. The generated shock wave then couples with the ignition and transits into detonation at t_4 = 731.9 μs. Two pressure peaks are observed at t_4. The first small peak indicates the flame front, and the

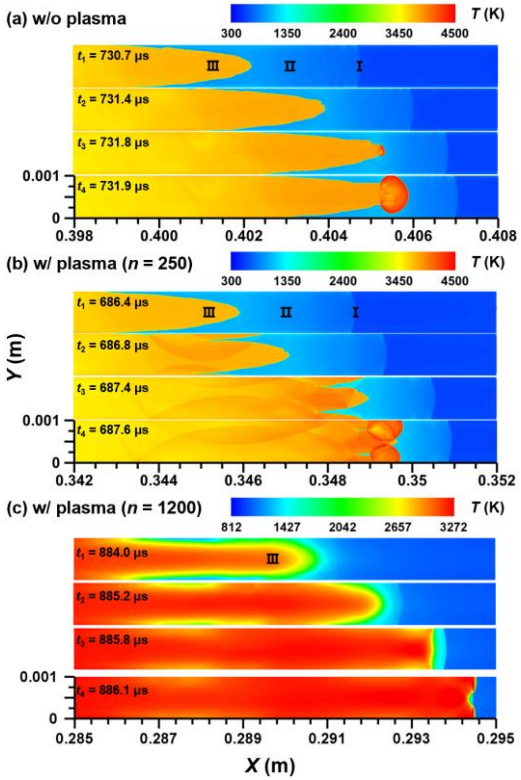

Fig. 4. Time evolutions of temperature (T) during DDT of the cases (a) without plasma, (b) with pulse numbers n = 250, and (c) n = 1200 (I: shock wave zone; II: induction zone; III: reaction zone).

second one indicates the autoignition and ignition-induced shock. The time evolution of Mach number also shows that the DDT initiation occurs when the reaction front propagates with a Mach number larger than 1. It is noted that the Mach number decreases at the flame front and then increases with autoignition occurrence at t_4 = 731.9 μs in Fig. 5(a). This is caused by the backward propagation of the ignition-induced shock.

For the DDT acceleration with the pulse number of 250, Fig. 4(b) shows that the DDT is initiated at the boundary layer which is formed due to the plasma-enhanced reactivity and the viscous effects between the precursor shock and the wall. To explain this, the time evolution of temperature at the bottom boundary is presented. Fig. 5(b) shows that the temperature in the boundary layer ahead of the flame is over 1000 K. At t_1 = 686.4 μs, similar to the no plasma case, a temperature gradient with increased reactivity (heat release rate) by plasma is generated in front of the flame at the boundary layer and the burned gas flow is choked. Although the plasma-enhanced reactivity is uniform across the channel, the interaction with viscous heating enhances the reactivity further at the

boundary layer. The plasma-generated species such as H_2O_2, O_3, $H_2(v=1)$ induce new reaction pathways via $H_2O_2(+M) = 2OH(+M)$, $O_3(+M) = O + O_2(+M)$, $O + H_2(v=1) \rightarrow H + OH$ and $H_2(v=1) + OH \rightarrow H_2O + H$. The radical production accelerates the fuel oxidation and heat release rate at the boundary (see Fig. 5(b)), promoting localized autoignition. Therefore, the autoignition first occurs at the top and bottom boundaries instead of the flame front, as shown at t_2 = 686.8 μs in Fig. 4(b). Then, the ignition propagates downstream by spontaneous ignition sequences and forms an ignition wave (t_3 = 687.4 μs). This ignition propagation results in more heat release in the boundary layer, which further increases the temperature ahead of the ignition front and enhances the reactivity gradient. Therefore, the ignition front accelerates and approaches the precursor shock. Meanwhile, the compression waves are generated continuously and increase the pressure correspondingly. At t_4 = 687.6 μs, Fig. 4(b) shows that the ignition front with a strong reactivity gradient develops into a strong shock wave. The heat release, temperature, and pressure increase significantly at the shock front. The two shock waves at the top and bottom boundaries merge and initiate detonation.

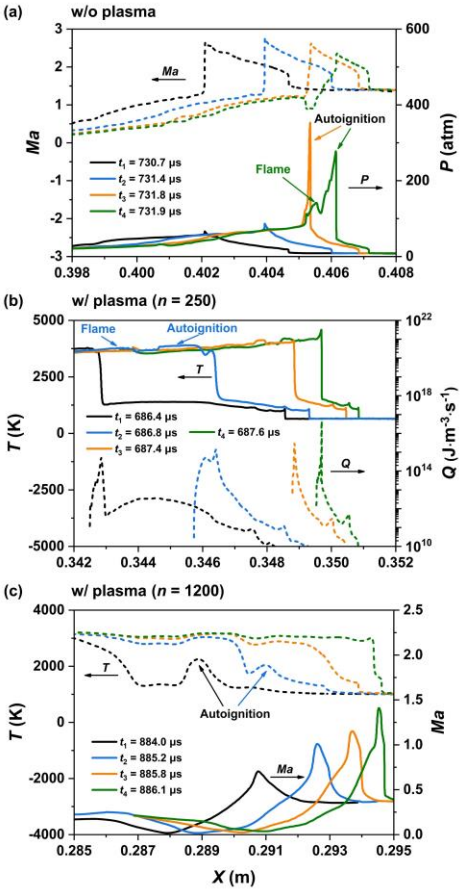

Fig. 5. Time evolutions of (a) Mach number (*Ma*) and pressure (*P*) at the centerline of the channel without plasma; (b) temperature (*T*) and heat release (*Q*) at the bottom boundary with n = 250; and (c) temperature at the bottom boundary and Mach number at the centerline with n = 1200. The centerline and the bottom boundary are marked in Fig. 1(a). Because DDT occurs at the centerline without plasma and at the boundaries with pulse number n = 250 and 1200, variables are plotted at the centerline without plasma and at the bottom boundary with n = 250 and 1200. The horizontal axis represents the coordinates at these locations. An exception is the Mach number for n = 1200, as the flow speed is zero at the non-slip boundary. The Mach number at the centerline for n = 1200 clearly demonstrates that the flow speed did not exceed the sound speed before DDT. (More information about *Ma*, *P*, *T*, and *Q* is provided in the Supplementary material)

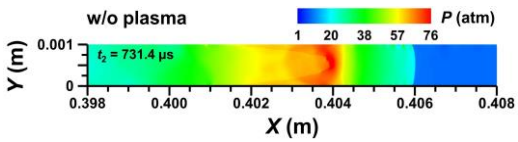

Fig. 6. Pressure during DDT without plasma at t_2 = 731.4 μs.

At n = 1200, the DDT also occurs at the boundary layer initiated by autoignition, however, without a leading shock wave and acoustic choking of the burned gas (see the Mach number in Fig. 5(c)). Fig. 5(c) shows that the autoignition occurs ahead of the flame at the boundary at t_1 = 884.0 μs, which takes a longer time compared with the DDT without plasma and with a pulse number of 250. Table 1 shows that an initial temperature of 810 K is achieved at n = 1200. Different from the heat release rate acceleration with plasma discharge number n = 250, the autoignition at n = 1200 is mainly caused by the elevated temperature and reactivity by a large number of plasma pulses and wall friction. Then the temperature and reactivity gradients are formed at the boundary layer, and the ignition wave is generated. The elevated temperature increases sonic velocity and the large amount of fuel consumption with more plasma pulse reduces the heat release rate of the mixture, making it more difficult for the leading shock to form and ignition-shock coupling. Without a leading shock, the pressure ahead of the flame fails to rise, and acoustic choking does not occur. It can be seen in Fig. 5(c) that a second autoignition occurs at t_2 = 885.2 μs. This supersonic ignition wave directly initiates DDT at t_3 = 885.8 μs when the Mach number is larger than 1 (Fig. 5c).

Figure 7 shows the pressure-specific volume (*P*-*V*) phrase diagram at different locations during DDT. The black solid and red dashed lines indicate the locations before DDT and at DDT, respectively. For location X_1, all three cases show similar trends. At the starting time, the normalized specific volume is unity for all cases. The mixture is first compressed by the compression waves produced by the flame acceleration, as shown by black curves from the unity volume to the turning point t_1 in Figs. 7(a) and (b) and t_2 in Fig. 7(c). This follows the shock Hugoniot curve

in which the specific volume decreases with the pressure increase. The first turning point indicates the arrival of flame at this location. Then, Figs. 7(a) and (c) show that the specific volume increases at a nearly constant pressure with flame propagation. After that, the pressure decreases due to thermal expansion in the

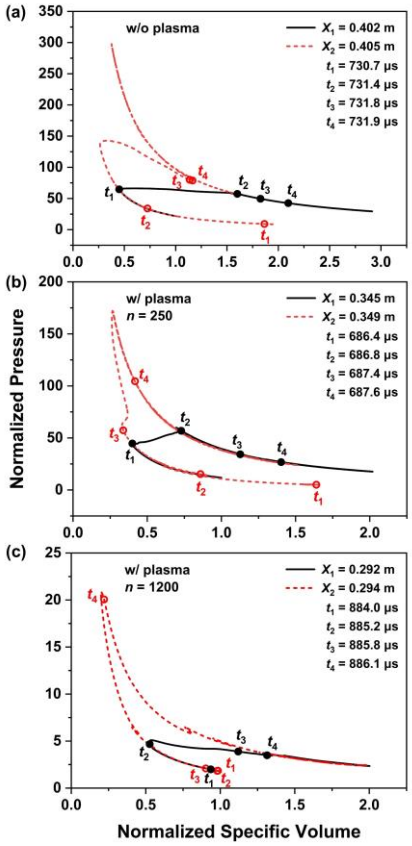

Fig. 7. Pressure-specific volume (*P-V*) phrase diagram at the locations before DDT (solid black line) and at DDT (dashed red line) (a) at the centerline without plasma, and at the bottom boundary with (b) n = 250 and (c) n = 1200.

reaction zone. Note that there is a pressure increase between t_1 and t_2 at n = 250 in Fig. 7(b). This is caused by the faster ignition wave propagation at the boundary shown in Fig. 4(b) due to plasma enhanced reactivity. For location X_2 without plasma, Fig. 7(a) shows that the pressure first increases to higher values due to the continuous compression between the flame and the precursor shock. After the flame front passes this location, the pressure decreases, as shown by the dashed red line between t_2 and t_3. Once the DDT occurs ahead of X_2 at t_4, the stronger shock wave propagates back to X_2, leading to the detonation. At n = 250, a stronger coupling between autoignition and shock wave is observed. The first turning point at t_3 in Fig. 7(b) indicates the autoignition occurrence. As a result, the specific volume and pressure increase simultaneously. After the ignition wave passes the X_2, a strong shock wave generated by the autoignition front arrives and results in the second turning point. At this point, the ignition wave begins to couple with the shock wave. This coupling is accelerated by the reactivity enhancement from plasma. Therefore, the peak shock wave pressure increases abruptly and results in faster DDT. In Fig. 7(c), with a pulse number of 1200, the first and second turning points shown in Fig. 7(b) disappear. This is because DDT is directly initiated by autoignition due to strongly accelerated reactivity and elevated temperature without burned gas choking. However, the absence of acoustic choking leads to a lower pressure rise and longer DDT onset time.

Figure 8 shows the comparison between flame/ignition velocity and local sonic velocity. The probe location is the same as the flame (or ignition) position and changes over time. The local sonic speed is calculated based on the local temperature (shown in Fig. S7 in the Supplementary material) and mixture compositions at the probe location. The results show that DDT only occurs when the ignition velocity (u_{ig}) exceeds the local sonic velocity (a) in all the cases. The gas pressure rise does not have enough time to equalize. The shock wave forms after transient evolution and transits to detonation. The numerical results clearly show that the occurrence of DDT follows by the Zel'dovich gradient mechanism [29]. Fig. 8(b) also shows that the ignition velocity first exceeds local sonic speed on the boundary, verifying that the DDT is initiated at the wall at n = 250.

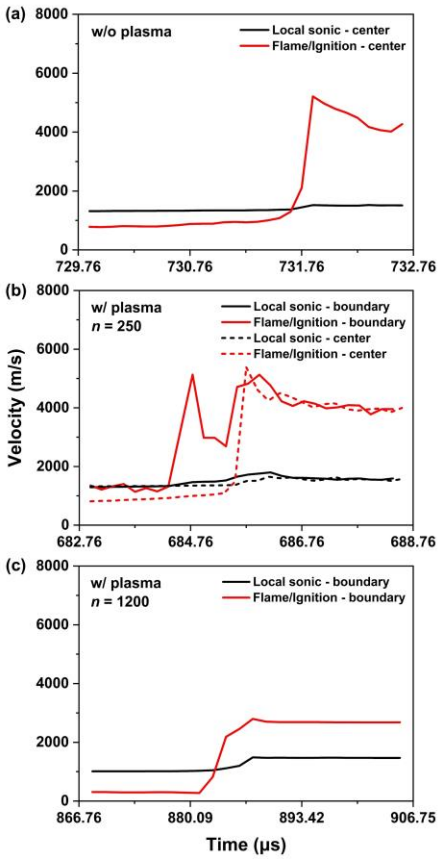

Fig. 8. Comparison between local sonic and flame/ignition velocity at the center and the bottom boundary (a) without plasma, (b) with 250 pulses, and (c) with 1200 pulses.

The plasma assisted DDT mechanism can be summarized in Figure 9. Without plasma discharge, the pressure and temperature gradients in front of the flame front are generated by acoustic compression. After the choking of the burned gas, the elevated pressure and temperature gradients initiate DDT via autoignition. With plasma discharge, there exist two different regimes, i.e., DDT initiation via acoustic choking of the burned gas at a small discharge pulse number and plasma-enhanced reactivity gradient without acoustic choking at a large discharge pulse number. With small pulse numbers, the plasma-generated species enhance the ignition kinetics. Coupled with non-uniformity created by viscous effects, a strong reactivity gradient is formed in the boundary layer. This advances the ignition wave propagation, ignition-shock wave coupling, and accelerates DDT after the acoustic choking of burned gas. With more plasma pulse numbers applied, the significant increase of mixture reactivity and elevated temperature by the excessive plasma assisted hydrogen oxidation trigger DDT via autoignition directly. DDT can occur without acoustic choking of the burned gas. Meanwhile, the DDT onset time is retarded because of the increased sonic velocity and lower heat release rate. As summarized by the discussion above, the DDT is initiated by autoignition in thermal, pressure, and reactivity gradients via Zel'dovich gradient mechanism both with and without plasma discharges.

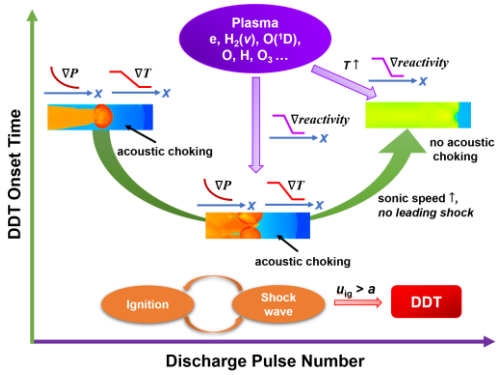

Fig. 9. Schematic of plasma assisted DDT mechanism.

4. Conclusions

The plasma assisted H_2/O_2 deflagration to detonation transition in a microscale channel is studied by numerical modeling with detailed chemistry and transport. The effects of nanosecond pulsed discharges on fuel oxidation and DDT dynamics are investigated. The results show that there exists a non-monotonic dependence between DDT onset time and discharge pulse number. The DDT is accelerated by a small discharge pulse number and the onset time is reduced by 44 μs. However, a large discharge pulse number retards the DDT onset by 154 μs. Two DDT regimes are observed with different discharge pulse numbers. One regime is that the DDT is initiated via acoustic choking of the burned gas at a small discharge pulse number. The other one is via plasma-enhanced reactivity gradient without acoustic choking at large pulse numbers. Without plasma discharge, the acoustic compression after the choking of the burned gas generates pronounced pressure and temperature gradients in front of the flame. DDT is triggered by these gradients via autoignition. For the DDT acceleration with small discharge pulse numbers, the DDT is accelerated due to the enhancement of autoignition sequences near the wall and ignition-shock wave coupling by the plasma-enhanced reactivity after the choking of the burned gas. The enhancement of ignition kinetics and increased reactivity in the boundary is contributed by the plasma-generated species such as H_2O_2, O_3, $H_2(v)$ via $H_2O_2(+M) = 2OH(+M)$, $O_3(+M) = O + O_2(+M)$, $O + H_2(v=1) \rightarrow H + OH$ and $H_2(v=1) + OH \rightarrow H_2O + H$. With a large discharge pulse number, the results show that DDT is initiated by a direct autoignition without the acoustic choking of the burned gas. This is attributed to the strongly accelerated reactivity and the resulting elevated temperatures by plasma discharges. However, the DDT onset is retarded

because the increased sonic velocity and the decrease of heat release rate prevent the formation of a leading shock and subsequent pressure buildup ahead of the flame. The modeling results also show that DDT is initiated by autoignition in thermal, pressure, reactivity field via Zel'dovich gradient mechanism both with and without plasma discharges. It is found that with strong plasma activation of a mixture, the acoustic choking of the burned gas is not a necessary condition for DDT with plasma-enhanced reactivity gradient. For future research, it is interesting to couple the plasma discharge and DDT processes together and investigate the effect of non-uniform plasma distribution across the channel on the DDT initiation [30].

Declaration of competing interest

The authors declare that they have no known competing financial interests or personal relationships that could have appeared to influence the work reported in this paper.

Acknowledgements

This project is supported by the DOE grant DE-SC0020233 of Plasma Science Center and NSF grant CBET 1903362. AT gratefully acknowledges the financial support of the Israeli Council for Higher Education - Planning and Budgeting Committee.

Supplementary material

The Supplementary material is submitted along with the manuscript.

References

[1] G.D. Roy, S.M. Frolov, A.A. Borisov, D.W. Netzer, Pulse detonation propulsion: challenges, current status, and future perspective, Prog. Energy Combust. Sci 30 (2004) 545-672.

[2] G. Ciccarelli, S. Dorofeev, Flame acceleration and transition to detonation in ducts, Prog. Energy Combust. Sci 34 (2008) 499-550.

[3] R. Zipf Jr, V. Gamezo, M. Sapko, W. Marchewka, K. Mohamed, E. Oran, D. Kessler, E. Weiss, J. Addis, F. Karnack, Methane–air detonation experiments at NIOSH Lake Lynn Laboratory, J. Loss Prevent. Proc. 26 (2013) 295-301.

[4] R.W. Houim, A. Ozgen, E.S. Oran, The role of spontaneous waves in the deflagration-to-detonation transition in submillimetre channels, Combust. Theor. Model. 20 (2016) 1068-1087.

[5] M.-H. Wu, W.-C. Kuo, Accelerative expansion and DDT of stoichiometric ethylene/oxygen flame rings in micro-gaps, Proc. Combust. Inst. 34 (2013) 2017-2024.

[6] M. Ivanov, A. Kiverin, I. Yakovenko, M.A. Liberman, Hydrogen–oxygen flame acceleration and deflagration-to-detonation transition in three-dimensional rectangular channels with no-slip walls, Int. J. Hydrogen Energ. 38 (2013) 16427-16440.

[7] E.S. Oran, V.N. Gamezo, Origins of the deflagration-to-detonation transition in gas-phase combustion, Combust. Flame 148 (2007) 4-47.

[8] A.Y. Poludnenko, J. Chambers, K. Ahmed, V.N. Gamezo, B.D. Taylor, A unified mechanism for unconfined deflagration-to-detonation transition in terrestrial chemical systems and type Ia supernovae, Science 366 (2019) eaau7365.

[9] J. Sepulveda, A. Rousso, H. Ha, T. Chen, V. Cheng, W. Kong, Y. Ju, Kinetic enhancement of microchannel detonation transition by ozone addition to acetylene mixtures, AIAA J. 57 (2019) 476-481.

[10] J. Crane, X. Shi, A.V. Singh, Y. Tao, H. Wang, Isolating the effect of induction length on detonation structure: Hydrogen–oxygen detonation promoted by ozone, Combust. Flame 200 (2019) 44-52.

[11] Y. Ju, W. Sun, Plasma assisted combustion: Dynamics and chemistry, Prog. Energy Combust. Sci 48 (2015) 21-83.

[12] A. Starikovskiy, N. Aleksandrov, Plasma-assisted ignition and combustion, Prog. Energy Combust. Sci 39 (2013) 61-110.

[13] X. Mao, H. Zhong, Z. Wang, T. Ombrello, Y. Ju, Effects of inter-pulse coupling on nanosecond pulsed high frequency discharge ignition in a flowing mixture, Proc. Combust. Inst. 39 (2023) 5457-5464.

[14] A. Starikovskiy, N. Aleksandrov, A. Rakitin, Plasma-assisted ignition and deflagration-to-detonation transition, Philos. Trans. R. Soc. A 370 (2012) 740-773.

[15] A.A. Tropina, R. Mahamud, Effect of plasma on the deflagration to detonation transition, Combust. Sci. Technol. 194 (2022) 2752-2770.

[16] M. Vorenkamp, S.A. Steinmetz, T.Y. Chen, X. Mao, A. Starikovskiy, C. Kliewer, Y. Ju, Plasma-assisted deflagration to detonation transition in a microchannel with fast-frame imaging and hybrid fs/ps coherent anti-Stokes Raman scattering measurements, Proc. Combust. Inst. 39 (2023) 5561-5569.

[17] M. Vorenkamp, S. Steinmetz, X. Mao, Z. Shi, A. Starikovskiy, Y. Ju, C. Kliewer, Effect of Plasma-Enhanced Low-Temperature Chemistry on Deflagration-to-Detonation Transition in a Microchannel, AIAA J. 61 (2023) 4821-4827.

[18] X. Mao, A. Rousso, Q. Chen, Y. Ju, Numerical modeling of ignition enhancement of CH_4/O_2/He mixtures using a hybrid repetitive nanosecond and DC discharge, Proc. Combust. Inst. 37 (2019) 5545-5552.

[19] X. Mao, Q. Chen, A.C. Rousso, T.Y. Chen, Y. Ju, Effects of controlled non-equilibrium excitation on H_2/O_2/He ignition using a hybrid repetitive nanosecond and DC discharge, Combust. Flame 206 (2019) 522-535.

[20] Z. Wang, H. Zhao, C. Yan, Y. Lin, A.D. Lele, W. Xu, B. Rotavera, A.W. Jasper, S.J. Klippenstein, Y. Ju, Methanol oxidation up to 100 atm in a supercritical pressure jet-stirred reactor, Proc. Combust. Inst. 39 (2023) 445-453.

[21] W. Sun, Developments of Efficient Numerical Methods for Combustion Modeling with Detailed Chemical

Kinetics, Princeton University, Princeton, NJ, 2020 Ph.D. Dissertation.
[22] R. J. Kee, G. Dixon-Lewis, J. Warnatz, M. E. Coltrin, J. A. Miller, A Fortran Computer Code Package for the Evaluation of Gas-Phase Multicomponent Transport Properties, SAND-86-8246, Sandia National Labs., Livermore, CA, 1986.
[23] W. Sun, Y. Ju, A Multi-Timescale and Correlated Dynamic Adaptive Chemistry and Transport (CO-DACT) Method for Computationally Efficient Modeling of Jet Fuel Combustion with Detailed Chemistry and Transport, Combust. Flame 184 (2017) 297–311.
[24] X. Gou, W. Sun, Z. Chen, Y. Ju, A Dynamic Multi Timescale Method for Combustion Modeling with Detailed and Reduced Chemical Kinetic Mechanisms, Combust. Flame 157.6 (2010) 1111–21.
[25] K. H. Kim, C. Kim, O. Rho, Methods for the accurate computations of hypersonic flows: I. AUSMPW+ scheme, J. Comput. Phys. 174.1 (2001) 38-80.
[26] Farouk T, Farouk B, Staack D, Gutsol A, Fridman A, Modeling of direct current micro-plasma discharges in atmospheric pressure hydrogen, Plasma Sour. Sci. Technol. 16.3 (2007) 619.
[27] X. Mao, H. Zhong, N. Liu, Z. Wang, Y. Ju, Ignition enhancement and NOx formation of NH_3/air mixtures by non-equilibrium plasma discharge, Combust. Flame 259 (2024) 113140.
[28] D. Valiev, V. Bychkov, V. Akkerman, L. Eriksson, Different stages of flame acceleration from slow burning to Chapman-Jouguet deflagration, Phys. Rev. E 80.3 (2009) 036317.
[29] Y.B. Zeldovich, Regime classification of an exothermic reaction with nonuniform initial conditions, Combust. Flame 39 (1980) 211-214.
[30] S. Nagaraja, V. Yang, I. Adamovich, Multi-scale modelling of pulsed nanosecond dielectric barrier plasma discharges in plane-to-plane geometry, J. Phys. D: Appl. Phys. 46.15 (2013) 155205.